Available online at www.sciencedirect.com

SciVerse ScienceDirect

Ceramics International 39 (2013) 4961–4967

CERAMICS INTERNATIONAL

www.elsevier.com/locate/ceramint

Influences of infiltrated resin on properties of printed electrodes on non-sintered ceramic films

Youngwoo Kim[a], Kyoohee Woo[a], Jihoon Kim[b], Jooho Moon[a,*]

[a]Department of Materials Science and Engineering, Yonsei University, 50 Yonsei-ro Seodaemun-gu, Seoul 120-749, Republic of Korea
[b]Division of Advanced Materials Engineering, Kongju National University, 1224-24 Cheonan Daero, Chenan-si, Chungnam 331-717, Republic of Korea

Received 11 October 2012; accepted 27 November 2012
Available online 5 December 2012

Abstract

Ceramic–resin hybrid substrate-based printed capacitors are fabricated for next generation ceramic packaging. The resin solution is infiltrated into the non-sintered ceramic powder beds by either inkjet printing or spin-coating. The amount of infiltrated resin and its spatial distribution throughout the films critically influence the dielectric loss factor, the adhesion strength, and the electrical conductivity of the electrodes. Although inkjet printing leads to non-uniform distribution of the resin, spin-coating is an effective means to uniformly infiltrate the resin solution. The resulting non-sintering ceramic–resin hybrid substrate-based printed capacitors demonstrate optimal properties comparable to their state-of-the-art low-temperature co-fired ceramic (LTCC) counterparts.

Keywords: Ceramic–resin hybrid film; Film adhesion; Resin infiltration; Resistivity

1. Introduction

Extensive development of information technology drives wireless communication market demand for novel mobile electronic products with high performance, multiple functionalities, and small size. Such advanced electronic products require three-dimensional (3D) integration of hetero-materials on top of substrates [1–3]. Desirable properties for electronic package substrate materials include low dielectric loss, optimum relative permittivity, high thermal conductivity, constant coefficient of thermal expansion across active device materials, and excellent mechanical properties [4,5]. For this reason, a number of ceramic materials such as alumina (Al_2O_3), aluminum nitride (AlN) and zirconia (ZrO_2) have been investigated as candidate substrate materials [6–8]. However, conventional ceramic materials generally require high temperature sintering, a process by which the particles are transformed into consolidated matter, which may limit their use [9,10].

Recent years have seen the development of low temperature co-fired ceramics (LTCC) that are capable of integration into 3D systems by embedding active or passive components into ceramic substrates [11–13]. LTCC technology is compatible with low temperature processable Ag, Ni, or Cu conductive paste materials. However, it still requires process temperatures of 800–900 °C, which is too high for the integration of temperature-sensitive electronic devices such as organic-based materials and components. For this reason, ceramic hybrid materials consisting of ceramic particles filled with polymeric resin have been considered as a next generation substrate material for 3D electronic packaging systems because they have no need for high temperature sintering [14,15].

Inkjet printing can allow for direct patterning of various materials without the involvement of expensive fabrication processes. In particular, this method is suitable for fabrication of a multilayered 3D integrated package system due to accurate layer-to-layer alignment via direct circuit patterning. We previously demonstrated inkjet printing-based ceramic–resin hybrid substrate fabrication [16]. The alumina powder beds were produced by the inkjet printing of

*Corresponding author. Tel.: +82 2 2123 2855; fax: +82 2 312 5375.
E-mail address: jmoon@yonsei.ac.kr (J. Moon).

0272-8842/$ - see front matter © 2012 Elsevier Ltd and Techna Group S.r.l. All rights reserved.
http://dx.doi.org/10.1016/j.ceramint.2012.11.092

the alumina dispersion, and the resin was then infiltrated into the dried alumina powder bed. The conductive pattern was printed with Ag conductive ink on the resin-containing alumina powder beds. These processes were repeated until multilayered substrates were produced, followed by resin curing at 280 °C and Ag particle annealing at 250 °C. The resin infiltration process plays an important role in determining the electrical and mechanical properties of the resulting hybrid substrates [17–20]. The amount of infiltrated resin and its spatial distribution throughout the substrate critically affect the dielectric properties of a metal–insulator–metal (MIM) capacitor such as *Q*-value (total device quality factor reflecting signal losses from series resistances). They also influence the conductance of the printed Ag circuit as well as the conductive pattern quality. With these considerations, it is necessary to understand the resin infiltration process and its influence on the electrical and mechanical properties of the hybrid substrates. Here, we compare resin infiltration methods, i.e., spin-coating and inkjet printing, in terms of the dielectric and adhesion properties. The electrical property of the printed Ag electrode on a resin-infiltrated substrate was also investigated as a function of the infiltrated amount of resin. Our studies indicate that infiltration of the proper amount of resin and its uniform distribution are the most important factors for creating a high performance hybrid substrate.

2. Experimental method

2.1. Fabrication of resin-infiltrated ceramic hybrid substrate

To produce non-sintered powder beds, ceramic ink was prepared by dispersing Al_2O_3 powders (average particle size = 0.2 μm, Denka) in N,N-dimethylformamide (DMF) at a concentration of 8 vol%. The detailed experimental conditions are described in our previous report [16]. The formulated alumina inks were filtered through a 6 μm nylon mesh prior to use in order to remove agglomerates in the inks. A Pt-coated Si wafer was used as a bottom electrode for the dielectric property measurement. The UJ 200 inkjet printing unit (Unijet Co.) was equipped with a piezoelectric nozzle with a 50 μm orifice from Micro-fab technology. Single-layer printing produced alumina power beds with a thickness of 15 μm after drying at 80 °C. The packing densities of inkjet-printed alumina films were in the range of 55–60%. The resin infiltration was performed by either spin-coating or inkjet printing. The resin ink was prepared by dissolving cyanate ester in DMF solvent at a concentration of 24 vol%. The amount of the resin infiltrated by inkjet printing was accurately calculated based on the volume of the resin ink printed onto the power bed unit area, whereas estimating the resin amount was only possible when infiltrated by spin-coating. The obtained resin-infiltrated films were cured by near infrared (NIR) irradiation at 280 °C for 5 h. In order to create a top electrode of $4.0 \times 4.0\ mm^2$ for the electrical property measurements, Ag conductive ink (Advanced Nano Product Co.) was inkjet-printed onto the resin-filled alumina hybrid films. We fabricated the MIM capacitors using different infiltration methods and infiltrated resin amounts to understand their influences on the electrical and mechanical properties of the hybrid substrates. The printed Ag patterns were annealed at 250 °C for 1 h to develop electrical conductivity.

2.2. Characterizations

The mechanical integrity of the ceramic–resin hybrid substrates (without printed top Ag electrodes) was evaluated by an adhesion test (tape peel test method, ASTM D3359-2). 3 M scotch tape was applied to the film surface after removing all entrapped air, and the time between the application and removal of the tape was less than 1 min. The tape was removed by a rapid pull force applied perpendicular to the test area and was followed by analysis of the damaged area (%). The thickness of each layer was measured using a surface profilometer (Dektak 150, Veeco). The dielectric properties of the MIM capacitors were measured at 1 MHz by an impedance analyzer (Agilent 4294A) with a vertical type test fixture (HP 16034E). The sheet resistance of silver electrodes printed on top of the ceramic–resin hybrid substrates was measured by a four point probe (CMT-SR200N, Chang Min Co., Ltd.) as a function of the amount of infiltrated resin. All the resistances reported here reflected average values from more than five different regions. The cross-sectional microstructures of the MIM capacitors were analyzed by a field emission scanning electron microscope (FE-SEM, JSM-6700F, JEOL) and a confocal microscope (OLS3000, Olympus). The residual resin inside the substrate after curing was monitored by Raman spectroscopy (LabRam ARAMIS, Horiba Jobin-Yvon). To confirm the decomposition behavior of the cured resin, thermogravimetry coupled with differential scanning calorimetry (SDT Q600, TA Instrument Co., Ltd.) was utilized.

3. Results and discussion

3.1. Resin infiltration by inkjet printing

Fig. 1(a) shows schematics of all-inkjet-printing-based hybrid MIM capacitor fabrication: (a) the successive inkjet printings of alumina dispersion, resin solution, and silver conductive ink and (b) the electrical characterization of the resulting MIM capacitors after curing and annealing. SEM cross-sectional analysis revealed a homogenous hybrid film in which each layer has well packed and dense microstructures, as shown in Fig. 1(b) (inset). The thickness of the ceramic–resin film was about 15 μm, and the silver electrode was about 1.0 μm thick. The mechanical property of the ceramic–resin hybrid substrates was evaluated by an adhesion test as shown in Fig. 2. The white region in the film after the test indicated the intact area of the film,

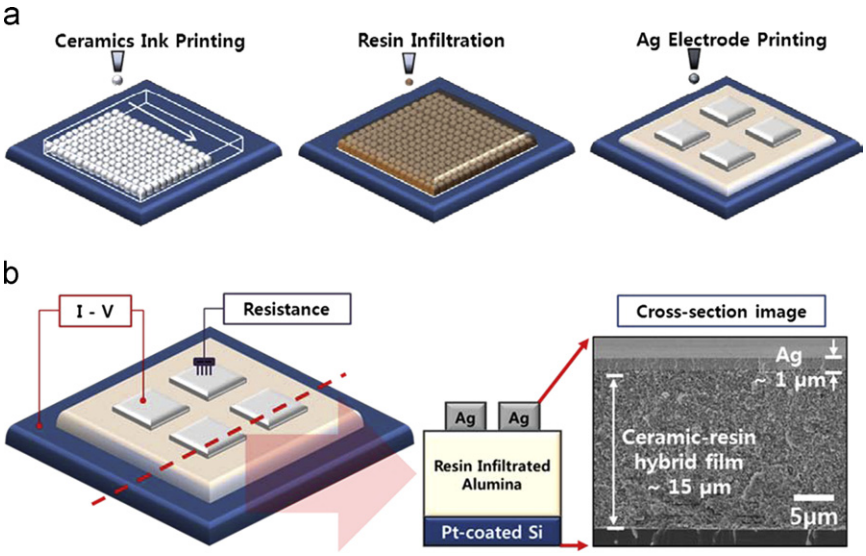

Fig. 1. Schematics of the all-inkjet-printing-based hybrid substrate fabrication process: (a) successive ink printings of alumina dispersion, resin and silver conductive ink, and (b) electrical characterization of the resulting MIM capacitor after curing/annealing. The cross-sectional microstructure of devices was analyzed by SEM. The thickness of the ceramic–resin hybrid film was about 15 μm, and that of the silver electrode was about 1.0 μm.

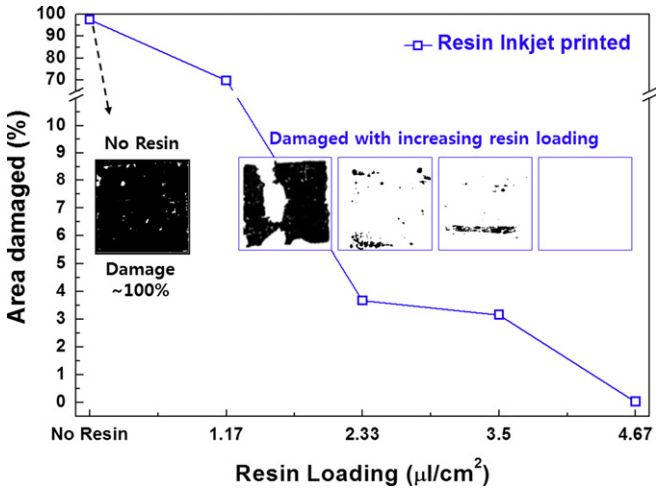

Fig. 2. The results of an adhesion test (ASTM D3359-2) for the ceramic–resin hybrid substrates fabricated by inkjet printing as a function of the infiltrated amount of resin after annealing. Optical images of the samples after the tape test are shown in the inset.

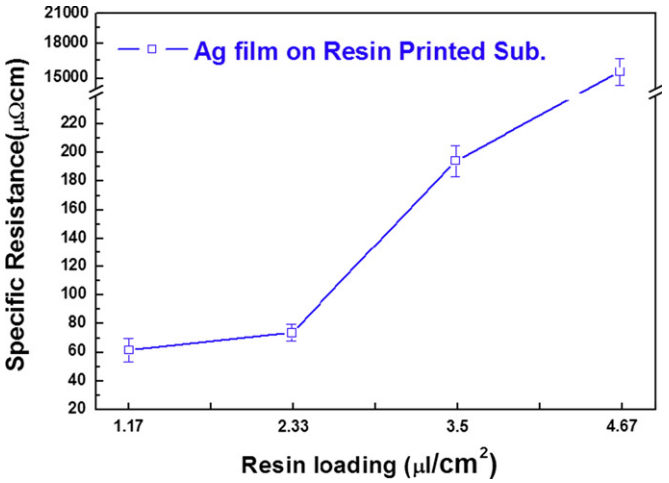

Fig. 3. Variation of the specific resistance of the annealed silver electrodes printed on ceramic–resin hybrid substrates in which different amounts of resin are pre-filled by inkjet printing.

whereas the black region reflected the area damaged (i.e., removed) by tape detachment. The ceramic film with no resin infiltration showed extremely poor adhesion (left inset). The amount of resin ink infiltrated into the unit area was calculated based on the printing frequency, pitch between ink droplets, and individual droplet volume. With increasing resin loading, the adhesion properties of the hybrid ceramic films improved as visually distinguished by the increased area fraction of the white region. In our previous paper, we determined that the optimum resin loading from inkjet printing is about 1.17 μl/cm^2 for optimal dielectric properties when the MIM hybrid capacitor has a Q-value of 390. However, the adhesion test results indicate that the resin infiltration of 1.17 μl/cm^2 after printing is insufficient to satisfy the adhesion strength requirements of the ceramic–resin hybrid substrate. Printing with a larger amount of resin to ensure adhesion would diminish the dielectric properties of the resulting MIM capacitor [16].

Fig. 3 shows the specific resistance of silver electrodes printed on the resin-filled ceramic films after annealing at 250 °C. It should be noted that the electrical conductivity of silver electrodes is influenced by the amount of resin in the underlying hybrid substrate even though the resin was pre-infiltrated and cured prior to the Ag printing. The specific resistance increased with increasing resin loading and varied between 43.4 and 18,907.5 μΩ cm. This observation suggests that the amount of infiltrated resin is closely related not only to sufficient mechanical strength

and desirable dielectric properties of the hybrid films, but also to the development of highly conductive metal electrodes printed on the substrate. The electrical conductivity of metal electrodes is important for determining the total device quality factor in an electronic package system device. Therefore, it is necessary to understand the cause of electric conductivity decline and to optimize the resin-infiltration process.

The cross-sectional microstructure of MIM capacitors as a function of the infiltrated amount of resin was examined as shown in Fig. 4. The film densities of the Ag electrode varied depending upon the resin loading, indicative of different densification behavior, although the electrode patterns were printed and annealed under identical conditions using the same conductive ink. The Ag particles on the less resin-filled hybrid substrate underwent adequate densification, whereas those on the more resin-filled hybrid substrate were not well-sintered, lowering the electrical conductivity of the silver electrode. The initial film microstructure of the electrode might be affected by the infiltrated amount of resin. Filling the micro-voids between Al_2O_3 particles with cyanate ester likely modifies the surface characteristics of the powder beds, which could alter the wettability and solvent penetration kinetics. When printing Ag ink onto a resin-filled substrate, different ink-substrate interactions may lead to the formation of a less densely packed structure for the patterned electrodes.

The initial microstructure of the granular film is a critical factor to determine the sintered microstructure of the Ag electrode, so that the less densely packed structure would be a reason for lower electrical conductivity in the case of the electrode printed on the more resin-filled substrate [21,22]. We examine the initial microstructure of the as-printed silver films prior to annealing, as shown in Fig. S1 (Supplementary information). The particle-packing structure of the silver particles and the surface geometry of the ceramic hybrid substrate were almost indistinguishable regardless of the amount of resin infiltrated. This observation excludes the possibility of microstructural alterations induced by the ink–substrate interactions and in turn suggests that electrical resistivity degradation occurs during annealing of the printed silver electrodes.

To confirm the influences of infiltrated resin on the sintering behavior of silver electrodes printed on ceramic–resin hybrid substrate, we performed cross-sectional Raman spectroscopic analysis as shown in Fig. 5. A focused laser with a beam size of 0.5 μm was scanned across the cross-section of the printed electrode-substrate (see the insets). The regions where the Raman spectra were obtained are marked in the optical image. For this analysis, two types of silver electrodes were printed on the glass substrate as well as on the ceramic hybrid substrate, followed by annealing at 250 °C, to investigate the influence of resin diffusion. No noticeable peak in the Raman spectrum (green line) was observed in the case of the annealed silver electrode on glass, indicating that any residual organic components contained in the Ag conductive ink were undetectable by Raman analysis. However, the spectrum (red line) obtained from the annealed Ag printed on the ceramic hybrid substrate exhibited similar peaks as those that appear in the ceramic hybrid substrate

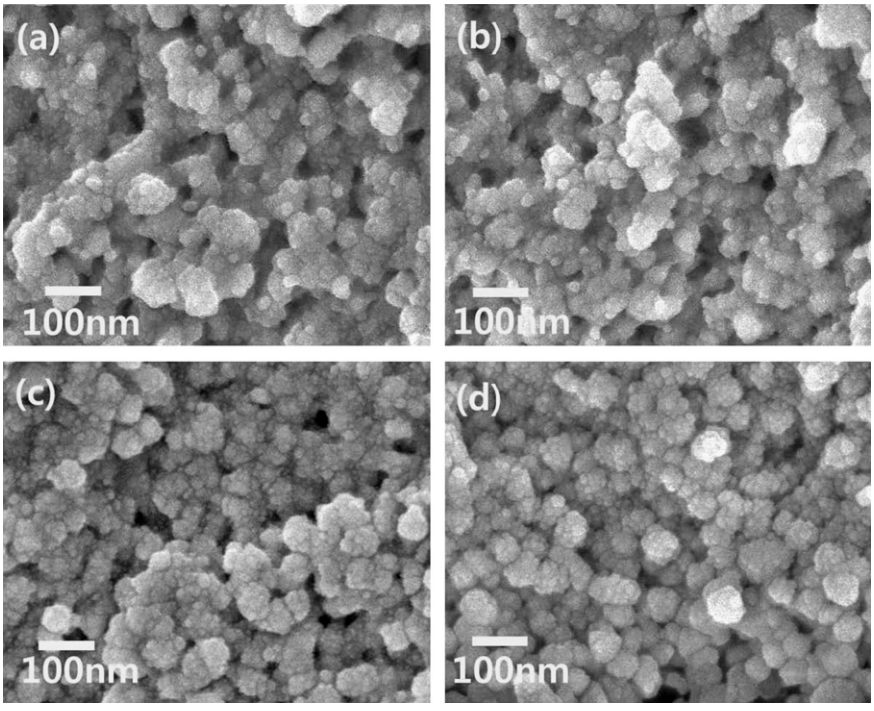

Fig. 4. Cross-sectional microstructure images of the annealed silver electrodes located near hybrid substrates in which different amounts of resin were pre-filled: (a) 1.17 μl/cm^2, (b) 2.33 μl/cm^2, (c) 3.50 μl/cm^2, and (d) 4.67 μl/cm^2.

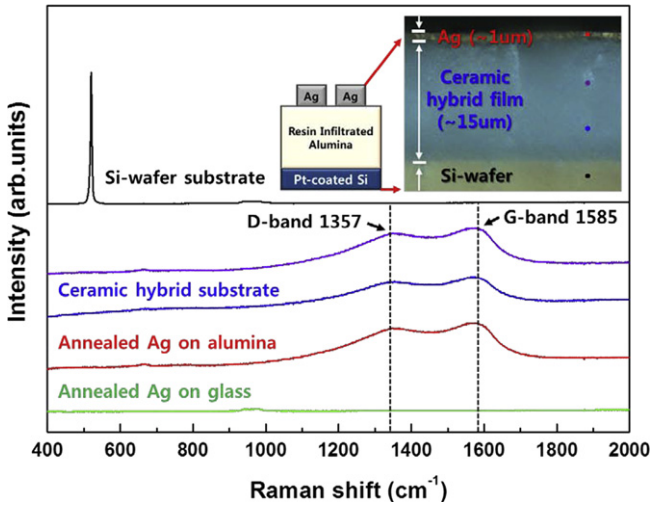

Fig. 5. Cross-sectional Raman spectroscopic analysis for the MIM capacitors fabricated on different substrates. Raman spectrum (green line) in the case of the annealed silver electrode on glass. The spectrum (red line) obtained from the annealed Ag printed on the ceramic hybrid substrate exhibits similar peaks as those that appear in the ceramic hybrid substrate (blue and purple lines). The points where the Raman spectra were obtained are marked in the optical image (inset). (For interpretation of the references to color in this figure legend, the reader is referred to the web version of this article.)

(blue and purple lines). The spectrum contains two primary features at 1357 cm^{-1} ("D-band") and 1585 cm^{-1} ("G-band"). The G-band corresponds to C–C stretching that is common to all sp^2-bonded carbons, while the D-band reflects disorder in the structure of the carbons [23,24]. This observation suggests that carbon-containing species are present in the Ag electrode printed on the ceramic hybrid substrate, and they originate from the decomposed resin by upward diffusion during the annealing process of silver electrodes. These carbon-containing species might adversely affect the sintering of Ag particles, leading to a less densely structured electrode with less electrical conductivity.

We analyzed thermal decomposition behavior of the cured resin by thermogravimetry coupled with differential scanning calorimeter (TG-DSC) to confirm its decomposition at the electrode annealing temperature (250 °C), as shown in Fig. 6. The cured resin began to lose weight at 200 °C, followed by an abrupt loss at 350 °C (Fig. 6(a)). To precisely determine the thermal decomposition behavior, we performed isothermal analysis of the cured resin at 250 °C, as shown in Fig. 6(b). The cured resin showed 3% weight loss within 3 h, indicating that the decomposed species in the substrate could diffuse upward into the printed electrode during the annealing process. Partial or incomplete decomposition of the cured cyanate ester likely leaves behind hydrocarbon impurities during annealing at 250 °C. These impurities can diffuse into the Ag particles, hindering effective mass transfer and preventing the particles from consolidating to form larger grains [25]. The

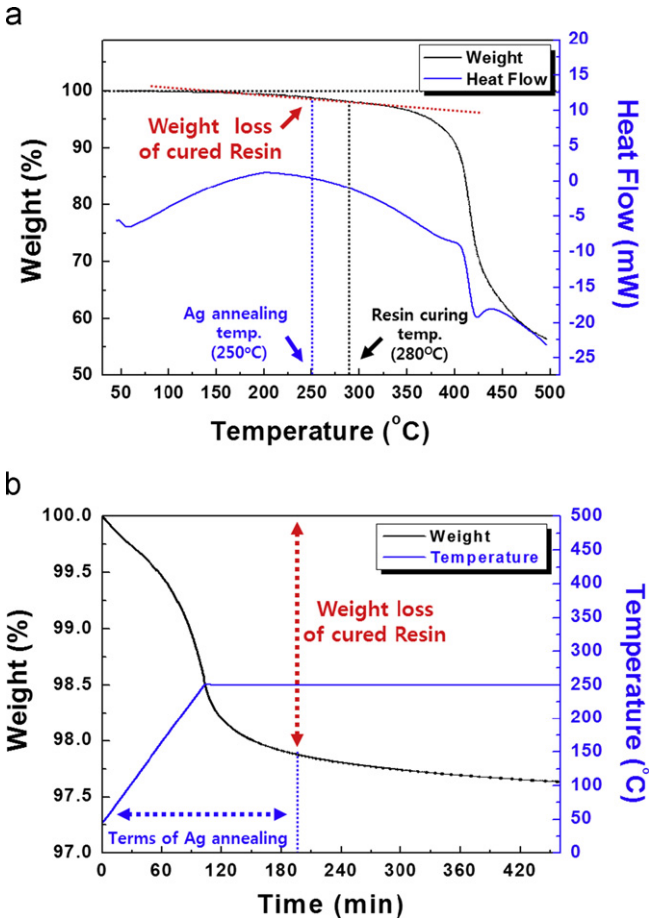

Fig. 6. (a) Thermogravimetry coupled with differential scanning calorimetry (TG-DSC) of the resin powder after curing at 280 °C for 5 h and (b) isothermal analysis of the cured resin at 250 °C.

residue of insulating hydrocarbon impurities would also contribute to the increase in the resistivity of the electrode.

3.2. Resin infiltration by spin-coating

As described above, inkjet-based resin printing is ineffective for fabricating a ceramic–resin hybrid substrate with good dielectric and electrical properties as well as sufficient mechanical strength. We need to find another resin-infiltration method that enables us to uniformly distribute the optimized amount of resin into ceramic powder beds. The hybrid substrate should have good adhesion strength, and the resulting MIM capacitor should have both a high Q-value and highly conductive electrodes. Problems with resin inkjet printing may be associated with drop-wise deposition. The initial droplets printed may penetrate and/or evaporate readily, whereas the droplets printed adjacent to the initial ones will experience slow penetration and/or evaporation. This different penetration/evaporation between the droplets of the resin inks causes a non-uniform resin distribution throughout the substrates after drying, which makes it difficult to optimize resin infiltration using inkjet printing.

We tried a spin-coating method in place of inkjet printing since the resin ink deposited onto the ceramic powder bed could evaporate at nearly the same time, allowing for more uniform resin distribution. Uniform resin distribution is easily discernible by visual inspection of the resin-filled alumina powder beds, as shown in Fig. S2 (Supplementary information). Fig. 7 shows the Q-values of the MIM capacitor fabricated by a resin spin-coating method as a function of resin loading. Only the resin infiltration process was replaced with spin-coating, while all other layers were produced under identical conditions. We used the same amount of resin loading as those in the inkjet printing methods (Figs. 2–4). It should be noted that resin loading reflects the initial amount of resin ink deposited onto the powder bed by a micropipette prior to spinning. The resin solution was dropped to cover the entire surface of the powder beds to allow infiltration. The resin ink might be drained off during spinning, which would alter the deposited resin amount from those in inkjet printing methods. The Q-value of the MIM capacitors fabricated by spin-coating becomes saturated at around 300. Although this value is lower than that of an inkjet printing-based MIM capacitor (Q-value = 390), it is comparable to the commercially available LTCC green sheets used for the electronic package substrates [14–16].

To confirm the mechanical properties, an adhesion test was performed on the ceramic–resin hybrid films fabricated by spin-coating, as shown in Fig. 8. The ceramic–resin hybrid film apparently needed less resin loading to ensure suitable mechanical properties as compared with those made by inkjet printing. The films containing more than 1.17 μl/cm^2 of resin survived the tape peel test without damage. Good adhesiveness can be attributed to uniform distribution of the resin throughout the film without local segregation. Need for less resin after spin-coating may also allow a highly conductive electrode to be formed on top of the ceramic–resin hybrid substrate.

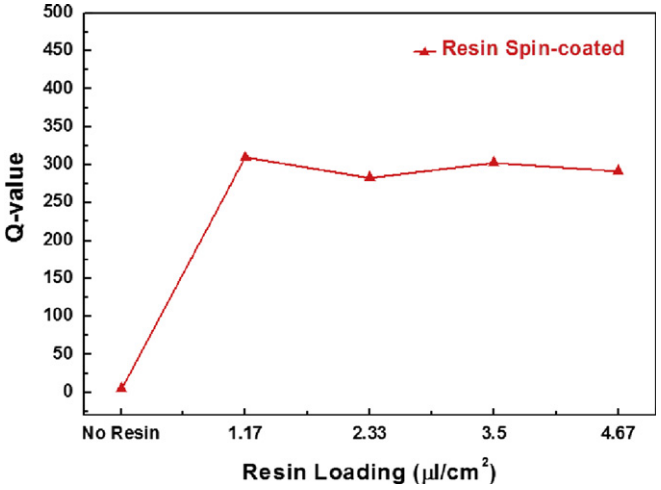

Fig. 7. Q-value (the inverse of loss tangent) of the MIM capacitors fabricated by a spin-coating method as a function of the amount of resin. Only the resin infiltration process was replaced with spin-coating, while all the other layers were produced under identical conditions. It should be noted that the resin loading parameter reflects the initial amount of resin ink deposited onto the powder bed by a micropipette prior to spinning.

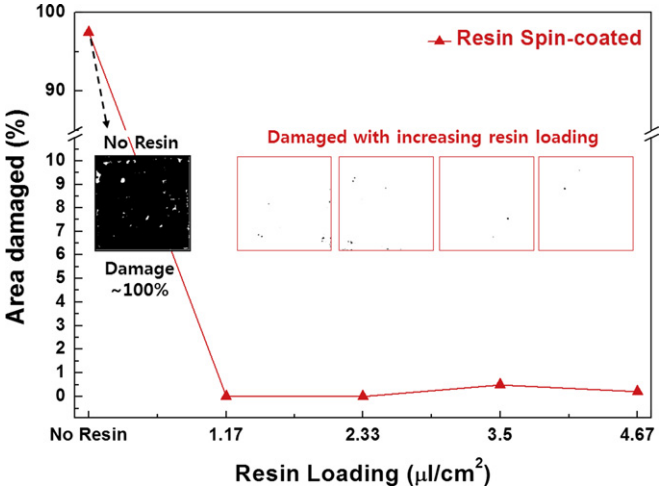

Fig. 8. The results of an adhesion test (ASTM D3359-2) for the ceramic–resin hybrid substrates fabricated by spin-coating as a function of the apparent amount of resin after annealing. Optical images of the samples after the tape test are shown in the inset.

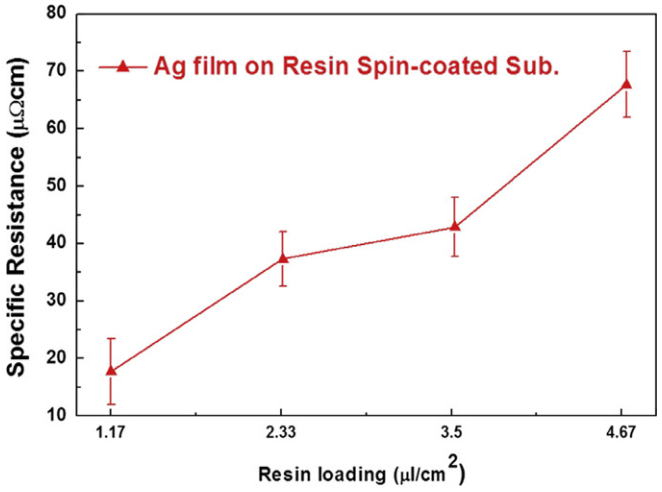

Fig. 9. Variation in the specific resistance of the annealed silver electrodes printed on ceramic–resin hybrid substrates in which different apparent amounts of resin were pre-filled by spin-coating.

Fig. 9 shows the specific resistance of silver electrodes printed on the resin spin-coated hybrid substrates after annealing, as a function of the apparent amount of resin. Although the electrical conductivity of silver electrodes printed on the resin spin-coated ceramic hybrid substrate also decreased with increasing resin loading, the conductivity remained much higher than that observed for the resin inkjet-printed substrates. The specific resistance was in the range of 17.9–67.9 μΩ cm. This observation clearly suggests that spin-coating allows for more uniform distribution of the resin.

4. Conclusions

We investigated the influences of infiltrated resin on the electrical and mechanical properties of the ceramic–resin hybrid substrate-based printed capacitors. The resin solution was infiltrated into the non-sintered alumina powder beds by either inkjet printing or spin-coating. The amount of infiltrated resin and its spatial distribution throughout the substrate play important roles in determining the dielectric loss factor, the adhesion strength, and the electrical conductivity of the electrodes. Drop deposition associated with inkjet printing led to non-uniform penetration/evaporation of the resin solution, which resulted in a non-uniform distribution of the resin, degrading the *Q*-value and the film adhesiveness. The cured resin infiltrated into the power beds, decomposed and diffused upward to the overlying printed electrode during its annealing process. It is suspected that the diffused hydrocarbon-based impurities hindered the Ag particles of the electrode from sintering and thereby deteriorated the electrical conductivity of the annealed Ag electrode. Resin solution deposition by spin-coating allows for uniform distribution of the resin at the minimized amount, during which the non-sintering ceramic–resin hybrid-based printed capacitor exhibits optimized properties, comparable to state-of-the art LTCC-based counterparts.

Acknowledgments

This work was supported by the National Research Foundation of Korea (NRF) grant funded by the Korean government (MEST) (Nos. 2012R1A3A2026417 and 2011-8-2048). It was also partly supported by the Second Stage of the Brain Korea 21 Project.

Appendix A. Supporting information

Supplementary data associated with this article can be found in the online version at http://dx.doi.org/10.1016/j.ceramint.2012.11.092.

References

[1] M.B. Tian, Substrates for High Density Package Engineering, Tsinghua University Press, Beijing, 2003, pp. 22–24.
[2] I.J. Youngs, G.C. Stevens, A.S. Vaughan, Journal of Physics D: Applied Physics 39 (2006) 1267–1276.
[3] R.R. Tummala, Journal of American Ceramic Society 74 (1991) 895–908.
[4] J.D. Bolt, D.P. Button, B.A. Yost, Materials Science and Engineering:A 109 (1989) 207–211.
[5] M.T. Sebastian, G. Subodh, C. Pavithran, P. Mohanan, Journal of the European Ceramic Society 27 (2007) 3039–3044.
[6] K. Park, S.Y. Lee, S. Kim, J. Chang, S.J.L. Kang, K.J. Leez, Electrochemical and Solid-State Letters 13 (2010) 57–59.
[7] T.S. Jeon, J.M. White, D.L. Kwong, Applied Physics Letters 78 (2001) 368–370.
[8] M.A. Khan, M. Shatalov, H.P. Maruska, H.M. Wang, E. Kuokstis, Japanese Journal of Applied Physics 44 (2005) 7191–7206.
[9] K.S. Seol, H. Hiramatsu, Y. Ohki, I.H. Choi, Y.T. Kim, Journal of Materials Research 16 (2001) 1883–1886.
[10] Y. Zhu, J. Zhu, Y.J. Song, S.B. Desu, Applied Physics Letters 73 (1998) 1958–1960.
[11] Y. Imanaka, Multilayered Low Temperature Cofired Ceramics (LTCC) Technology, Springer, New York, 2003, pp. 4–13.
[12] M.R. Gongora-Rubio, P. Espinoza-Vallejos, L. Sola-Laguna, J.J. Santiago-AvileÂs, Sensors and Actuators A 89 (2001) 222–241.
[13] C.W. Tang, C.Y. Chang, IEEE MTT-S Digest 3 (2002) 2201–2204.
[14] F. Xiang, H. Wang, X.J. Yao, Journal of the European Ceramic Society 26 (2006) 1999–2002.
[15] A.A. Okhlopkova, E.Y. Zhou, Mechanics of Composite Materials 40 (2004) 145–150.
[16] M.S. Hwang, J. Kim, H.T. Kim, Y. Yoon, S. Hyun, J. Kim, S.N. Lee, J. Moon, Journal of Applied Physics 108 (2010) 102809.
[17] D.H. Yoon, J. Zhang, B.I. Lee, Materials Research Bulletin 38 (2003) 765–772.
[18] S. Torquato, Random Heterogeneous Materials, Springer, New York, 2001, pp. 556–559.
[19] S.J. Penn, N.M. Alford, A. Templeton, X. Wang, M. Xu, M. Reece, K. Schrapel, Journal of the American Ceramic Society 80 (1997) 1885–1888.
[20] J. Mollá, M. Gonzalez, R. Vila, A. Ibarra, Journal of Applied Physics 85 (1999) 1727–1730.
[21] K.S. Chou, K.C. Huang, H.H. Lee, Nanotechnology 16 (2005) 779–784.
[22] L. Hu, H. Wu, Y. Cui, MRS Bulletin 36 (2011) 760–765.
[23] M.S. Dresselhaus, A. Jorio, M. Hofmann, G. Dresselhaus, R. Saito, Nano Letters 10 (2010) 751–758.
[24] K.S. Blinn, H. Abernathy, X. Li, M. Liu, L.A. Bottomley, M. Liu, Energy and Environmental Science 5 (2012) 7913–7917.
[25] Z.A. Peng, X. Peng, Journal of the American Chemical Society 124 (2002) 3343–3353.